

Rigid–Flexible Block Molecules Based on a Laterally Extended Aromatic Segment: Hierarchical Assembly into Single Fibers, Flat Ribbons, and Twisted Ribbons

Eunji Lee, Zhegang Huang, Ja-Hyoung Ryu, and Myongsoo Lee*^[a]

Abstract: Self-assembling rigid–flexible block molecules consisting of a laterally extended aromatic segment and different lengths of hydrophilic coils were synthesized and characterized. The block molecule based on a long poly(ethylene oxide) coil (**1**), in the melt state, shows an unidentified columnar structure, whereas the molecule with a shorter poly(ethylene oxide) coil (**2**) self-organizes into an oblique columnar structure. Further decrease in the poly(ethylene oxide) coil length as in the case of **3**, on heating, induces a rectangular columnar structure in addition to an oblique columnar mesophase. In

diethyl ether, **1** and **2** were observed to self-assemble into uniform nanofibers with bilayer packing. Remarkably, these elementary fibers were observed to further aggregate in a lateral way to form well-defined flat ribbons (**1**) and twisted ribbons (**2**) with solvent exchange of diethyl ether into methanol. Furthermore, the ribbons formed in methanol dissociated into elementary fibers in response to the addition of ar-

omatic guest molecules. This transformation between ribbons and single fibers in response to the addition of guest molecules is attributed to the intercalation of aromatic substrates within the rigid segments and subsequent loosening of the aromatic stacking interactions. These results demonstrate that the introduction of a laterally extended aromatic segment into an amphiphilic molecular architecture can lead to the hierarchical formation from elementary fibers of nanoribbons with a tunable twist through controlled lateral interactions between aromatic segments.

Keywords: amphiphiles • nanostructures • ribbons • self-assembly • solvent effects

Introduction

Precise control of a supramolecular nanostructure with a well-defined shape and size in self-organizing materials is of critical importance in acquiring a desired function and specific properties in the fields of molecular and supramolecular materials.^[1] Rigid aromatic rod segments are versatile building blocks for constructing such controlled nanoarchitectures.^[2,3] For example, incorporation of a rigid aromatic segment into amphiphilic molecular architectures with enhanced aggregation stability leads to a variety of nanostructures including barrels, toroids, helices, and tubes, depending on the molecular structure.^[4,5] Among them, one-dimensional helical structures have attracted much attention because

they are structurally comparable to peptide systems with the biological β -sheet motif. Peptides with a propensity towards β -sheet formation self-assemble into a hierarchy of twisted structures, from tapes to twisted ribbons with increasing solution concentration.^[6] In addition, a peptidomimetic self-assembles into various one-dimensional structures including filaments, helical fibrils, ribbons, and twisted ribbons, depending on solution pH.^[7] Inspired by such peptide assemblies, extensive efforts have been made to introduce helicity into artificial aromatic systems to construct twisted nanostructures. For example, dendron rod–coil molecules give rise to the transformation between high aspect ratio ribbon-like nanostructures and helical nanostructures triggered by the introduction of a chiral moiety.^[8] In addition, symmetrical and asymmetrical incorporation of flexible chiral coils into both ends of a π -conjugated aromatic segment leads to the formation of twisted and coiled helices, respectively.^[9]

Recently, we have shown that a rigid–flexible macrocyclic molecule consisting of a hexa-*p*-phenylene aromatic and a chiral poly(ethylene oxide) coil self-assembles into well-defined ribbonlike aggregates at an initial state which, in turn, roll up to form a helical tubular structure with a preferred

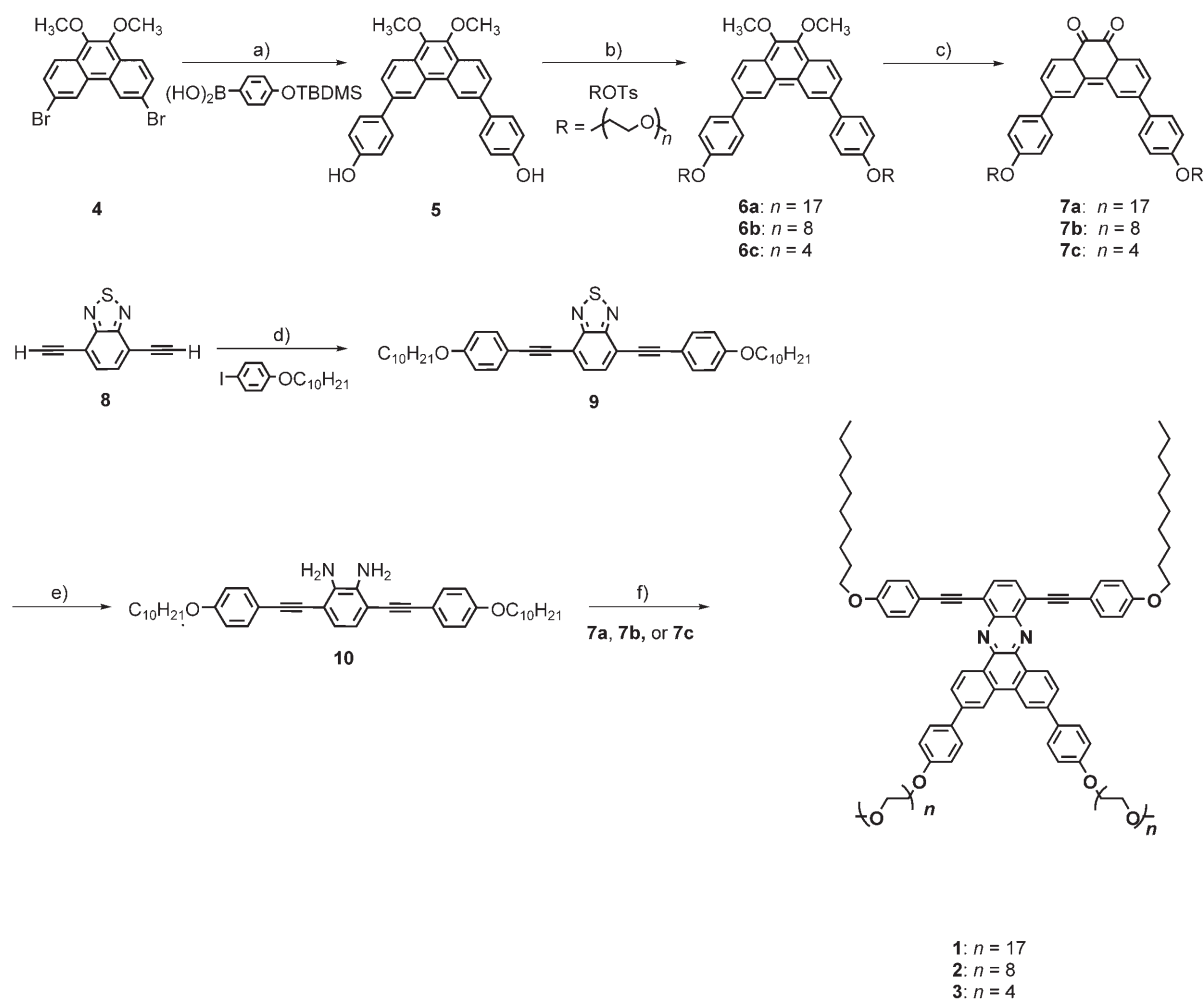
[a] E. Lee, Z. Huang, Dr. J.-H. Ryu, Prof. Dr. M. Lee
Center for Supramolecular Nano-Assembly
and Department of Chemistry
Yonsei University, Shinchon 134, Seoul 120-749 (Republic of Korea)
Fax: (+82)2-393-6096
E-mail: mslee@yonsei.ac.kr

Supporting information for this article is available on the WWW under <http://dx.doi.org/10.1002/chem.200800664>.

handedness.^[10] These helical strands are attributed to the energy balance between repulsive interactions among the adjacent flexible coils and π -stacking interactions. Although one-dimensional elementary structures have been extensively studied, the precise control of the hierarchical assembly of such elementary structures remains to be explored. One can envision that introduction of a laterally extended aromatic segment into amphiphilic molecules can give rise to hierarchical formation from elementary fibers to flat ribbons through enhanced lateral interactions between elementary structures. With this in mind, we have synthesized rigid-flexible block molecules consisting of a laterally extended aromatic segment and poly(ethylene oxide) (PEO) hydrophilic coils. We present herein the thermotropic liquid-crystalline phase behavior and hierarchical self-assembly behavior in solutions of the resulting amphiphilic rigid-flexible block molecules.

Results and Discussion

Synthesis: The rigid-flexible block molecules are based on a K-shaped rigid phenazine derivative containing decyl groups at lateral positions and hydrophilic poly(ethylene oxide) coils at the termini (Scheme 1). To synthesize the phenanthrenequinone aromatic scaffolds containing hydrophilic coils (**7**), precursor **4** was prepared according to procedures described previously.^[11a] Compound **5** was prepared from the Suzuki coupling reaction with **4** and a boronic acid derivative in the presence of Pd⁰ catalyst, and then the subsequent etherification with tosylated PEO coils afforded **6**. For the coupling reaction with the aromatic scaffolds containing hydrophobic coils, compound **7** was prepared in good yield by the cerium(IV) ammonium nitrate (CAN)-mediated reaction with **6**. The aromatic scaffold containing decyl groups (**10**) was synthesized by means of Sonogashira coupling with a benzothiadiazole derivative (**8**) and subsequent reduction with LiAlH₄. The final rigid-flexible block molecules were prepared by the condensation of the appropriate dione with **10**.^[11b,c] The resulting amphiphilic block



Scheme 1. Synthesis of the aromatic amphiphiles **1**, **2**, and **3**. a) Na₂CO₃, [Pd(PPh₃)₄], THF, reflux; b) K₂CO₃, acetonitrile, reflux; c) cerium(IV) ammonium nitrate (CAN), acetonitrile; d) [Pd(PPh₃)₄], CuI, Et₃N, THF, 60 °C; e) LiAlH₄, THF, reflux; f) acetic acid, ethanol.

molecules (**1**, **2**, and **3**) were characterized by ^1H and ^{13}C NMR spectroscopies, elemental analysis, and MALDI-TOF mass spectrometry, and shown to be in full agreement with the structures presented. As confirmed by ^1H NMR spectroscopy, the ratio of the protons of the aromatic block to the alkyl protons is consistent with the ratio calculated. The experimental mass based on peak positions in the spectrum is well matched with the theoretical molecular weight of each molecule (see the Supporting Information).

Liquid-crystalline behavior: The thermotropic liquid-crystalline phase behavior of the block molecules was investigated by means of differential scanning calorimetry (DSC), thermal optical polarized microscopy, and X-ray scatterings. Figure 1a reveals the DSC heating and cooling traces of the rigid-flexible block molecules. All of the molecules exhibit

thermotropic liquid-crystalline behavior after crystalline melting, and the transition temperatures and the corresponding enthalpy changes are summarized in Table 1. Molecule **1**, based on long PEO chains, melts into a birefringent liquid-crystalline phase that transforms into isotropic liquid at 89.3°C . On slow cooling from the optically isotropic phase, the formation of a fernlike texture that corresponds to a typical columnar mesophase takes place (see the Supporting Information). To confirm the two-dimensional symmetry of the columnar mesophase, X-ray scatterings have been performed at 80°C . However, the diffraction patterns showed only a strong single peak at the small-angle range together with a diffuse halo in the wide-angle region, which did not allow us to identify the columnar structure without ambiguity (Figure 2a).

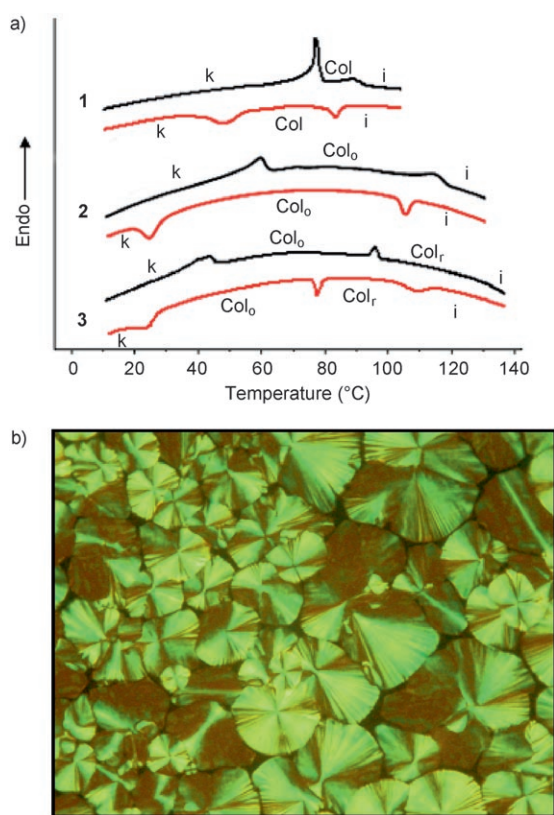


Figure 1. a) DSC traces recorded during the heating scan and cooling scan of aromatic molecules (k: crystalline phase; col_0 : oblique columnar phase; col_r : rectangular columnar phase; i: isotropic phase). b) Representative optical polarized micrograph of the texture exhibited by a columnar structure of **2** at the transition from the isotropic liquid state.

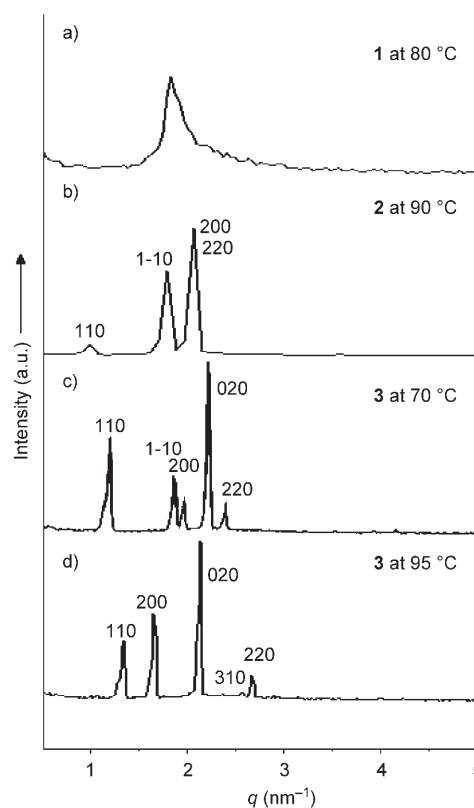


Figure 2. Small-angle X-ray diffraction patterns of **1–3** plotted against q . a) The pattern of the mesophase exhibited by **1** at 80°C , b) the oblique columnar lattice exhibited by **2** at 90°C , c) the oblique columnar lattice exhibited by **3** at 70°C , and d) the rectangular columnar lattice exhibited by **3** at 95°C .

Table 1. Thermal transitions of aromatic amphiphiles.^[a]

Molecules	$\rho^{[b]}$ [g cm^{-3}]	$f_{\text{PEO}}^{[c]}$	Calcd molecular length [nm]	Phase transition [$^\circ\text{C}$] and corresponding enthalpy changes [kJ mol^{-1}]	
				heating	cooling
1	1.24	0.62	7.3	cr 77.6 (6.6) col 89.3 (1.5)i	I 83.9 (1.2) col 48.8 (4.7) cr
2	1.12	0.45	4.9	cr 59.4 (6.1) col_0 114.5 (3.6)i	I 105.3 (3.1) col_0 24.4 (5.9) cr
3	1.08	0.31	3.7	cr 41.4 (3.6) col_0 91.5 (1.7) col_r 126.0 (0.1)i	I 103.1 (2.4) col_r 74.0 (1.9) col_0 22.5 (3.4) cr

[a] Data are from heating and cooling scans. cr: crystalline phase; col_0 : oblique columnar; col_r : rectangular columnar; i: isotropic phase. [b] ρ = molecular density. [c] f_{PEO} = volume fraction of PEO group to hydrophilic part.

Similarly, compound **2** based on short PEO chains also displays a columnar mesophase. After a crystal melting transition at 59.4°C, compound **2** exhibits a birefringent liquid-crystalline phase, followed by an isotropic phase at 114.5°C. Upon cooling from the isotropic liquid, a spherulitic fan texture can be observed by using an optical polarized microscope, characteristic of a columnar mesophase (Figure 1b). To corroborate the detailed liquid-crystalline structure of **2**, small- and wide-angle X-ray scattering experiments were performed at 90°C. The small-angle X-ray scattering (SAXS) of this mesophase displays three sharp reflections that can be indexed as a two-dimensional oblique columnar structure (a *P1* space group symmetry) with lattice constants $a=b=7.2$ nm and a characteristic angle of 60° (Figure 2b).^[12] The wide-angle X-ray scattering (WAXS) shows only a broad halo centered at approximately 4.5 Å, which is indicative of the liquid-crystalline order of aromatic segments within domains (see the Supporting Information).

To further confirm the formation of an oblique columnar structure, the sample was quickly quenched in liquid nitrogen after annealing at 90°C and then was cryomicrotomed to a thickness of approximately 50 to 70 nm. The microfilms of **2** were stained with RuO₄ vapor and observed by transmission electron microscopy (TEM). As shown in Figure 3,

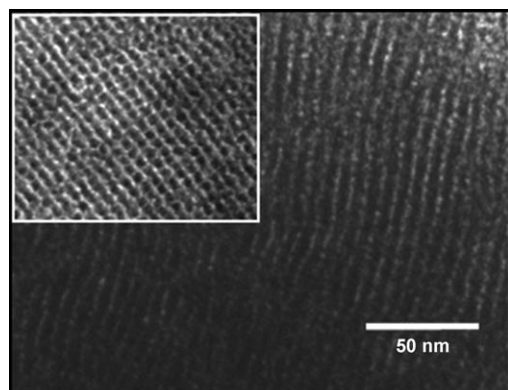


Figure 3. TEM images of ultramicrotomed films of **2** stained with RuO₄, revealing a columnar array of alternating light-colored flexible coils and dark aromatic layers. The inset image at perpendicular beam incidence shows an oblique columnar array of aromatic core.

the TEM image of **2** shows organized, darkly stained hydrophobic domains consisting of aromatic and alkyl segments with a thickness of around 6 nm. The inset TEM image shows in-plane order of an oblique symmetry in which dark hydrophobic domains are regularly arrayed in a matrix of light-colored coil segments. The interdomain distance was measured to be approximately 7.5 nm, which is consistent with that obtained from X-ray scattering. Interestingly, **3** exhibits an additional liquid-crystalline phase above a lower temperature mesophase (Figure 1a). On heating, compound **3** melts into a liquid-crystalline phase at 41.4°C, and then converts into a second liquid-crystalline phase, which in turn undergoes isotropization at 126.0°C. Similar to that of **2**, in

the lower temperature liquid-crystalline phase, the corresponding small-angle X-ray diffraction patterns show a number of well-resolved reflections, which can be indexed as a two dimensional oblique columnar lattice with lattice parameters $a=6.9$ nm, $b=6.1$ nm, and $\gamma=69^\circ$. On further heating to the second liquid-crystalline phase, the oblique columnar structure transforms into a rectangular columnar structure with lattice parameters $a=7.7$ nm, $b=6.0$ nm, and $\gamma=90^\circ$. Calculation based on the lattice constants and measured densities of both **2** and **3** reveals that the number of molecules in a single slice of the column is about four, indicating the same number of molecules per columnar cross section irrespective of the length of the PEO chain.^[13] Based on these results, the column can be considered to consist of three distinct molecular regions that result from the micro-segregation of the flexible chains from the rigid aromatic segments.^[14] The alkyl chains in the core are surrounded by aromatic segments arranged in a square shape, which are held together by means of the hydrophobic interaction of alkyl chains, whereas hydrophilic PEO chains in the periphery are filled with the intercolumnar matrix (Figure 4).

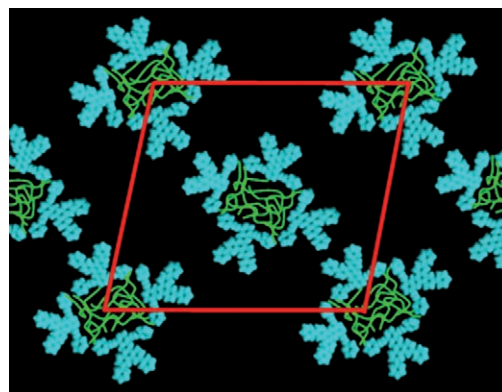


Figure 4. Schematic representation of the self-assembly of **2** ($a=7.2$ nm, $b=7.2$ nm, and $\gamma=60^\circ$) and **3** ($a=6.9$ nm, $b=6.1$ nm, and $\gamma=69^\circ$) into a two-dimensional columnar structure with an oblique lattice (alkyl chains in green, aromatic segments in blue, PEO coil matrix in black).

Aggregation behavior in solution: The rigid-flexible block molecules, when dissolved in a solvent suitable for the oligo(ethylene oxide) segments, can self-assemble into an aggregation structure due to their amphiphilic characteristics.^[15] The aggregation behavior was subsequently investigated with **1** and **2**, which show good solubility in polar solvents. Dynamic light scattering (DLS) experiments performed in diethyl ether, a selective solvent of the PEO chains, showed that both molecules aggregate into nanostructures with a monomodal size distribution, which indicates well-equilibrated structures (Figure 5a).^[16] The average hydrodynamic radii (R_H) of **1** and **2** were observed to be approximately 160 and 110 nm, respectively. TEM micrographs of both molecules showed fibrous aggregates with uniform diameters of 11 and 7 nm for **1** and **2**, respectively (Figure 5b and c). The extended molecular lengths are 7.3 and

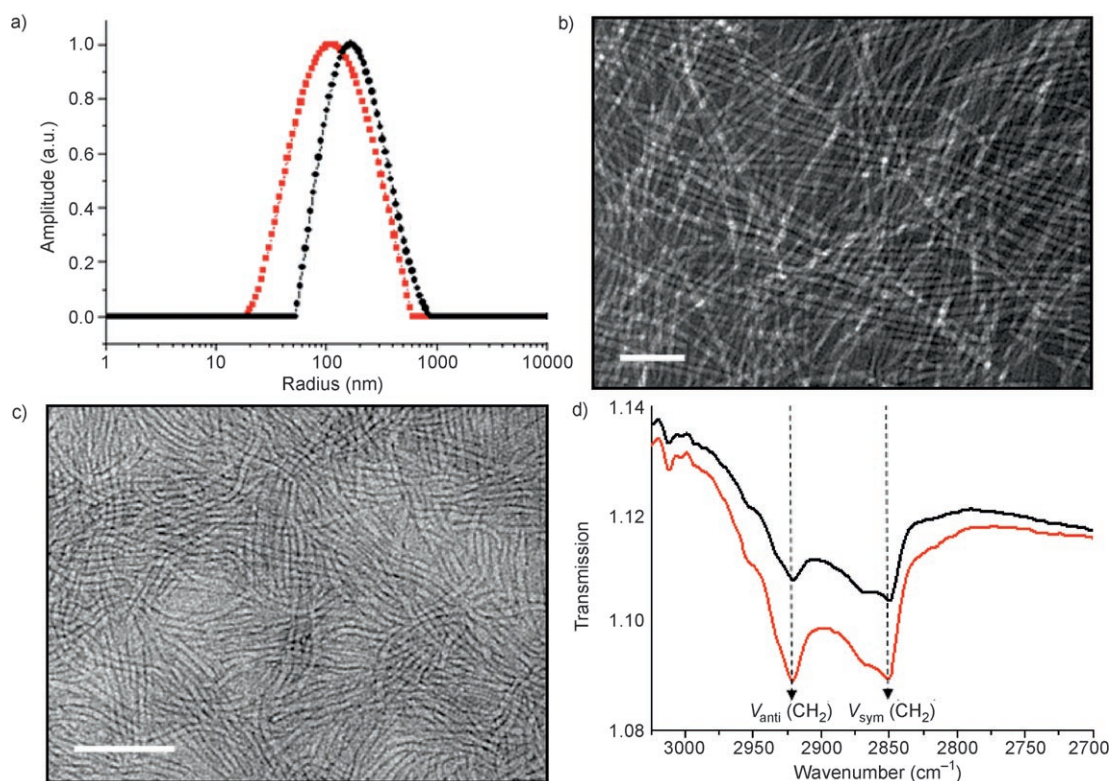


Figure 5. a) Size distribution graphs of **1** (—) and **2** (—) in diethyl ether at a scattering angle of 90°C (from CONTIN analysis of the autocorrelation function; 0.1 wt %). TEM images of b) **1** and c) **2** in diethyl ether (scale bars: 100 nm; 0.01 wt %). d) FTIR spectra ($2700\text{--}3025\text{ cm}^{-1}$) of solutions of self-assembled **1** in methanol (—) and diethyl ether (—).

4.9 nm for **1** and **2** (by CPK: Corey–Pauling–Koltun), respectively; these widths are consistent with an interdigitated bilayer packing of the hydrophobic segments. The bilayer feature is also reflected in FTIR spectroscopic experiments (Figure 5d). The films of **1** and **2** cast from solutions in diethyl ether showed two bands at 2918 cm^{-1} (ν_{anti}) and 2850 cm^{-1} (ν_{sym}), which contribute to modes corresponding to CH_2 stretching vibrations in the crystalline packing of alkyl chains.^[17] These results suggest that the fibrous aggregates consist of hydrophobic aromatic segments and decyl alkyl groups in the core surrounded by poly(ethylene oxide) coils that are exposed to the diethyl ether environment. Within the core, the extended aromatic segments are stacked in a bilayer packing arrangement (Figure 6).

We expected that replacing diethyl ether with methanol, which is a poorer solvent for ethylene oxide coils, would strengthen hydrophobic and $\pi\text{--}\pi$ stacking interactions between aromatic segments.^[18] The fluorescence spectrum of **1** in diethyl ether ($4 \times 10^{-4}\text{ M}$) exhibits a strong emission maximum at 525 nm without any noticeable fluorescence quenching (Figure 7b), which suggests that the aromatic segments within aggregates in diethyl ether are loosely packed. However, the emission maximum in methanol ($4 \times 10^{-4}\text{ M}$) is red-shifted with respect to that observed in chloroform, and fluorescence is significantly quenched, which indicates that strong $\pi\text{--}\pi$ stacking interactions between the aromatic segments are induced upon exchange of the solvent into metha-

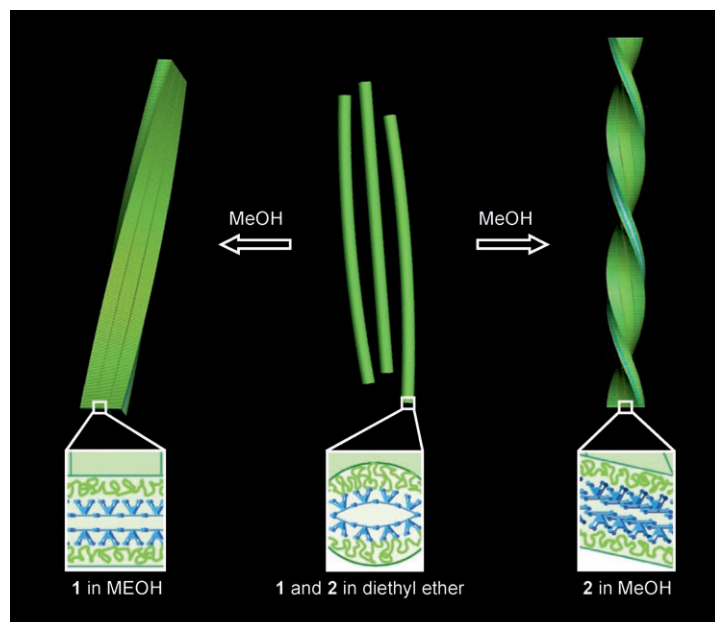


Figure 6. Schematic representation of the transformation from nanofibers to flat ribbon or twisted ribbon in response to solvent exchange.

anol.^[18,19] The fluorescence experiments with a solution of **2** in methanol exhibit a similar optical behavior, which indicates that the aromatic segments of **2** also pack closely to

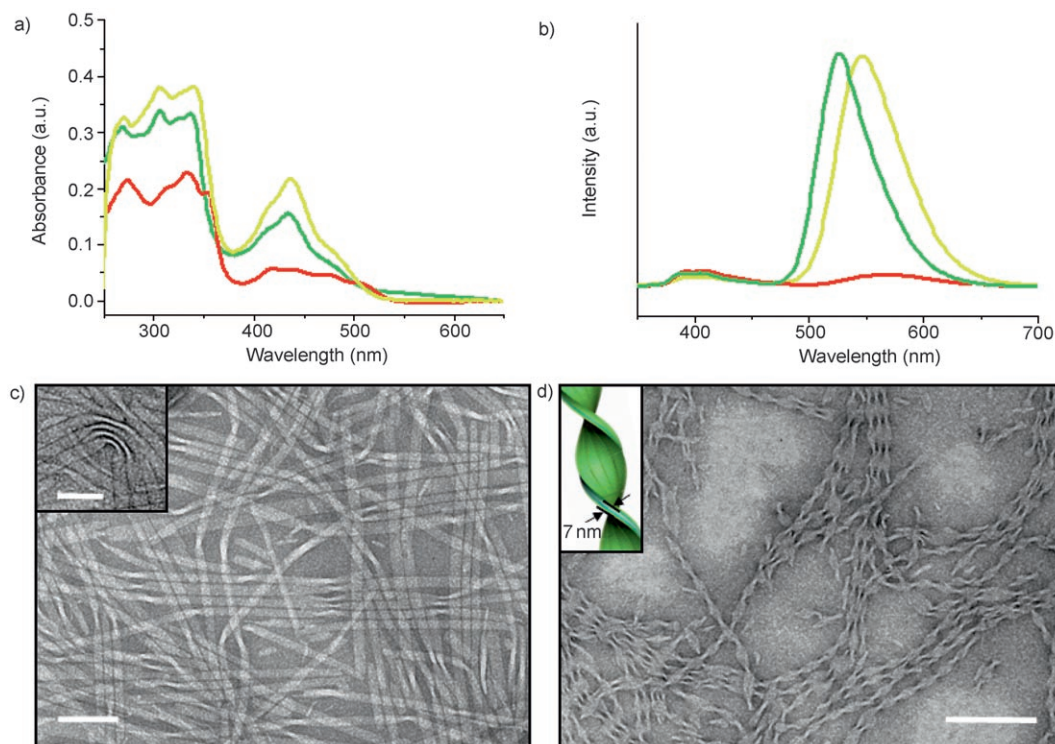


Figure 7. a) Absorption and b) emission spectra of molecule **1** in methanol (—) and diethyl ether (—) compared with chloroform (—) ($c=4 \times 10^{-4}$ M; $l=10$ mm; $\lambda_{\text{ex}}=295$ nm). c) TEM image of the flat ribbonlike aggregates of **1** in methanol (0.01 wt %; scale bar: 200 nm; inset: thickness of ribbon, scale bar: 100 nm). d) TEM image of the twisted ribbons of **2** in methanol with negative staining (0.01 wt %; scale bar: 200 nm).

each other through enhanced π - π interactions in methanol (see the Supporting Information).

TEM investigations of **1** cast onto a TEM grid from a solution in methanol showed one-dimensional strands with an average width of approximately 30 nm (Figure 7c). Close examination of the objects revealed the folded edges of individual strands with a thickness of 11 nm (Figure 7c, inset). This dimension is consistent with the expected thickness of interdigitated bimolecular packing (11 nm), clearly indicating a ribbonlike shape. Based on these results, aromatic amphiphile **1** can be concluded to self-assemble into a flat ribbon structure with a width of 30 nm and a thickness of 11 nm. These dimensions suggest that the elementary fibers based on bimolecular packing are laterally associated into stacks of three fibers to produce flat ribbons with solvent exchange from diethyl ether to methanol. This result clearly demonstrates that strong π - π interactions enhance the aggregation characteristics of the laterally extended aromatic amphiphiles, which results in the hierarchical formation of the ribbons.

In contrast, the elementary fibers of **2** transform into twisted ribbons with solvent exchange of diethyl ether into methanol. As shown in Figure 7d, the TEM micrograph reveals similar flat, ribbonlike structures to those of **1** in methanol, but with a regular twist about their long axis. The dimensions of the twisted ribbons were shown to be approximately 20 nm in width, around 7 nm in cross-sectional thickness, and with a pitch length of about 125 nm. Considering

the fully extended molecular length of 4.9 nm, the ribbon thickness of 7 nm indicates interdigitated bimolecular packing of the hydrophobic segments. This was further confirmed by FTIR spectroscopy that shows characteristic bands associated with bilayer packing of hydrophobic segments (see the Supporting Information).^[17] Considering that the fibers formed in diethyl ether have a width of 7 nm, the ribbons with a width of 20 nm consist of three laterally assembled elementary fibers. These results suggest that aromatic amphiphile **2** self-assembles at the initial stage into elementary fibers with a bilayer thickness; these further self-assemble in a hierarchical way through side-by-side hydrophobic interactions between the fibers into twisted ribbons.

Considering that **1** self-assembles into nontwisted, flat ribbons, the formation of twisted ribbons in **2** seems to be attributed to enhanced steric constraints imposed by closer packing of K-shaped aromatic segments. The molecule with longer poly(ethylene oxide) coils would be arranged into flat ribbons with bilayer packing as in the case of **1**. However, a decrease in the PEO length drives the K-shaped aromatic segments to be packed more closely due to reduced steric crowding of the PEO coils that are located at the ends of the ribbons. To fit more closely together, the aromatic segments are aligned with each other in a slight tilting arrangement, and consequently, the tilted stacks of the aromatic segments lead to the formation of twisted ribbon (Figure 6).^[20] This packing consideration of the aromatic segments is reflected in the increased extent of fluorescence

quenching in **2** compared with that of **1**, which implies that the π - π stacking interaction increases as the volume fraction of the PEO coil decreases (Figure 8).

To gain further insight into the role of the packing arrangement of the aromatic segments on the twisted ribbon, intercalation experiments of **1** and **2** have been performed with hydrophobic dye, Nile Red. The intercalation of the

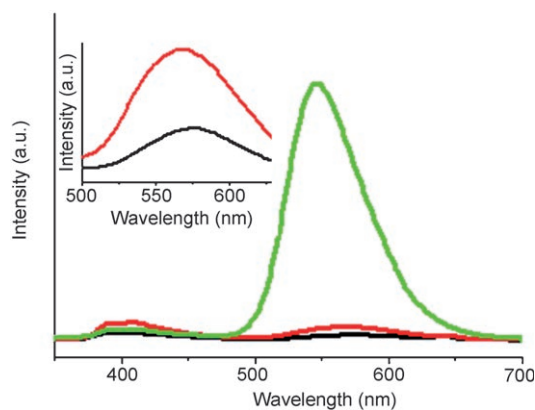


Figure 8. Emission spectra of molecule **1** (—) and **2** (—) in methanol compared with chloroform (—) ($c = 4 \times 10^{-4}$ M; $l = 10$ mm; $\lambda_{\text{ex}} = 325$ nm).

dye molecules between the aromatic segments in the ribbons would disrupt packing constraints imposed by close packing of K-shaped aromatic segments. The intercalation of Nile Red was confirmed by using fluorescence microscopy (Figure 9a). When the solution of **1** in methanol containing Nile Red was excited at 266 nm, the fluorescence intensity of **1** was suppressed while exhibiting strong emission at 624 nm corresponding to Nile Red due to energy transfer, clearly indicating that the guests are efficiently intercalated between the aromatic segments to interrupt π - π stacking interactions.^[9c,21] This packing frustration between the aromatic segments of the molecules would drive the ribbons to be dissociated into smaller aggregates. Upon addition of Nile Red, indeed, the flat ribbons were shown to transform into single fibers with a uniform diameter of approximately 11 nm (Figure 9b). Considering that the diameter of the ribbons formed in methanol is about 30 nm, the ribbons are dissociated into three elementary fibers upon addition of aromatic guest molecules. This result indicates that the flat ribbons of **1** are composed of three lateral stacks of elementary fibers, suggesting that the block molecules self-assemble, in a hierarchical fashion, into flat ribbons from single fibers. This transformation between ribbons and single fibers in response to the addition of guest molecules is attributed to the

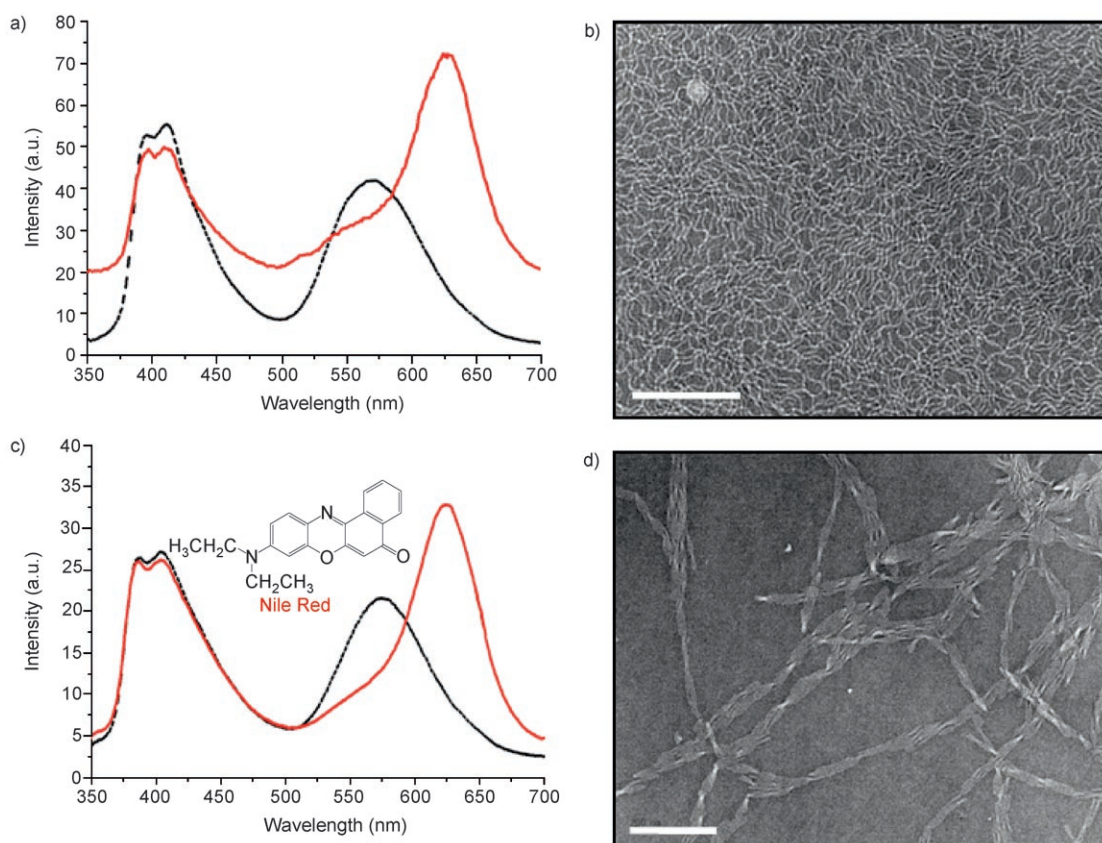


Figure 9. a) Emission spectra of a solution of **1** (---; $c = 4 \times 10^{-4}$ M) and of a solution of **1** and Nile Red (—; $c = 4 \times 10^{-4}$ M; 20 mol% relative to **1**; $\lambda_{\text{ex}} = 266$ nm). b) TEM image of **1** (0.01 wt %) containing 0.2 equiv of Nile Red (scale bar: 200 nm). c) Emission spectra of a solution of **2** (---; $c = 4 \times 10^{-4}$ M) and of a solution of **2** and Nile Red (—; $c = 4 \times 10^{-4}$ M; 20 mol% relative to **2**; $\lambda_{\text{ex}} = 266$ nm). d) TEM image of **2** (0.01 wt %) containing 0.2 equiv of Nile Red (scale bar: 200 nm).

intercalation of aromatic substrates within the rigid segments and subsequent loosening of aromatic stacking interactions. Upon addition of Nile Red, compound **2** also showed similar optical behavior to **1** (Figure 9c). TEM showed that **2** containing Nile Red forms flat ribbons together with a few irregular twists (Figure 9d). Instead, the ribbons are split into \approx three elementary fibers at irregular intervals. This result indicates that packing constraints of the K-shaped aromatic segments imposed by strong π - π stacking interactions are primarily responsible for the regular twisting of the flat ribbons.

Conclusion

Self-assembling rigid-flexible block molecules consisting of a laterally extended aromatic segment and different lengths of PEO coils were synthesized, and their self-assembling behavior in both bulk and solution was investigated. In the melt state, the rigid-flexible block molecule based on a long PEO coil (**1**) was observed to self-assemble into an unidentified columnar structure, whereas the molecule with shorter PEO coils (**2**) self-organizes into an oblique columnar structure. Further decrease in the PEO coil length as in the case of **3**, on heating, gives rise to transformation from an oblique columnar to a rectangular columnar structure. In diethyl ether, both **1** and **2** self-assemble into a fibrous structure with bilayer packing. Notably, these elementary fibers were observed to further aggregate in a lateral way to form flat ribbons with solvent exchange of diethyl ether into methanol. Decreasing the PEO length as in the case of **2** forces the flat ribbons to be curved to form twisted ribbons with a regular pitch along their axis due to steric constraints caused by enhanced π - π stacking interactions. Another interesting point to be noted is that the ribbons are dissociated into elementary fibers in response to addition of aromatic guest molecules due to interruption of π - π stacking interactions. Consequently, the incorporation of a laterally extended aromatic segment into an amphiphilic system provides a unique strategy to construct elementary fibers that further self-assemble into well-defined nanoribbons with a tunable twist. This result, which provides the precise control of hierarchical assembly, may have significant impact on the design of controlled one-dimensional supramolecular structures with electro-optical functions.

Experimental Section

Materials: *p*-Toluenesulfonyl chloride (98%) from Tokyo Kasei was used as received. Poly(ethylene glycol) methyl ether ($M_w = 350, 750$), 1,2-phenylenediamine (99.5%), phenanthrenequinone (95%), bromine, *n*-butyllithium (1.6 M solution in *n*-hexane), triisopropyl borate (98%), 4-iodophenol (99%), ammonium cerium(IV) nitrate (98.5%), and 1-bromodecane (98%) from Aldrich were used as received. Tetrakis(triphenylphosphine)palladium(0) and tetraethylene glycol monomethyl ether (98%) from TCI, and the conventional reagents were used as received. Visualization was accomplished with UV light and iodine vapor. Flash chroma-

tography was carried out with silica gel 60 (230–400 mesh) from EM science.

Techniques: ^1H NMR spectra were recorded from samples in CDCl_3 or DMSO by using a Bruker AM 250 spectrometer. The purity of the products was checked by thin-layer chromatography (TLC; Merck, silica gel 60). A Nikon Optiphot 2-pol optical polarized microscope (magnification: 100 \times) equipped with a Mettler FP 82 hot-stage and a Mettler FP 90 central processor was used to observe the thermal transitions and to analyze the anisotropic texture. A Perkin-Elmer DSC-7 differential scanning calorimeter equipped with a 1020 thermal analysis controller was used to determine the thermal transitions, which were reported as the maxima and minima of their endothermic or exothermic peaks. In all cases, the heating and cooling rates were $5^\circ\text{C}\cdot\text{min}^{-1}$. X-ray scattering measurements were performed in transmission mode using synchrotron radiation at the 10C1 X-ray beam line at Pohang Accelerator Laboratory, Korea. Microanalyses were performed using a Perkin-Elmer 240 elemental analyzer at the Organic Chemistry Research Center, Sogang University, Korea. MALDI-TOF mass spectrometry was performed by using a Perseptive Biosystems Voyager-DE STR with 2,5-dihydroxybenzoic acid as matrix. DLS measurements were performed by using an ALV/CGS-3 Compact Goniometer System. UV/Vis absorption spectra were obtained from a Shimadzu 1601 UV spectrometer. The fluorescence spectra were obtained from a Hitachi F-4500 fluorescence spectrometer. FTIR spectra were recorded by using an Equinox 55 FTIR spectrophotometer with a ZnSe pellet. TEM was performed at 120 kV by using a JEOL-JEM 2010 instrument. Compounds were synthesized according to the procedure described in Scheme 1 and then purified by silica gel column chromatography and preparative HPLC. Recycling preparative HPLC was performed at room temperature by using a 20 mm \times 600 mm polystyrene column on a Japan Analytical Industry Model LC-908 recycling preparative HPLC system, equipped with UV detector 310 and RI detector RI-5. Chloroform (HPLC grade) was used as eluent.

TEM: For the study of the self-assembled structure of K-shaped aromatic molecules in solution, a drop of solution of amphiphilic molecules was placed on a carbon-coated copper grid and the solution was allowed to evaporate under ambient conditions. The samples were stained by depositing uranyl acetate onto the surface of the sample-loaded grid. The dried specimen was observed by using a JEOL-JEM 2010 instrument operating at 120 kV. The data were analyzed using Digital Micrograph software.

Fluorescence spectroscopy: To investigate the co-assembled system of the K-shaped molecule and Nile Red, the prepared Nile Red solution ($1.0 \times 10^{-3}\text{ M}$) was added to **1** ($4.0 \times 10^{-4}\text{ M}$ in methanol) with a 0.2 ratio, [Nile Red]/[**1**], and fluorescence spectroscopy measurements were performed. Molecule **2** was also characterized using the same procedure.

DLS spectroscopy: DLS measurements were performed by using a UNIPHASE He-Ne laser operating at 632.8 nm. The scattering was kept at 90° during the whole experiment. The maximum operating power of the laser was 30 mW. The detector optics employed optical fibers coupled to an ALV/SOSIPD/DUAL detection unit, which employed an EMI PM-28B power supply and ALV/PM-PD preamplifier/discriminator. The signal analyzer was an ALV5000/E/WIN multiple-tau digital correlator with 288 exponentially spaced channels. The hydrodynamic radius (R_H) was determined from the DLS autocorrelation functions by the cumulants and the CONTIN methods by using the software provided by the manufacturer.

FTIR spectroscopy: Samples were prepared by dissolving an appropriate amount of aromatic amphiphiles in methanol (or diethyl ether), and then several drops of solution were coated on a ZnSe tablet.

Synthesis: The synthetic procedure used in the preparation of the K-shaped molecules is described in Scheme 1. Compounds **4** and **8** were synthesized according to the procedures described previously.^[11]

Synthesis of compound 5: Compound **4** (1.6 g, 4.04 mmol) and 4-(tetrabutyltrimethylsilyloxy)phenylboronic acid (2.55 g, 10.1 mmol) were dissolved in degassed THF (25 mL). Degassed 2 M aqueous Na_2CO_3 (25 mL) was added to the solution and then tetrakis(triphenylphosphine)palladium(0) (5 mg, 0.004 mmol) was added. The mixture was heated at reflux for 24 h with vigorous stirring under nitrogen, cooled to room temperature, the layers were separated, and the aqueous layer was then washed twice with

dichloromethane. The combined organic layer was dried over anhydrous magnesium sulfate and filtered. The solvent was removed with a rotary evaporator, and the crude product was purified by column chromatography (silica gel) using ethyl acetate to yield a yellow solid (1.7 g, 99%). $^1\text{H NMR}$ (250 MHz, CDCl_3): $\delta=8.74$ (s, 2H; ArH), 8.19 (d, $J=8.5$ Hz; 2Ar-H), 7.75 (d, $J=8.5$ Hz; 2Ar-H), 7.62 (d, $J=8.3$ Hz, 4H; m to OH), 7.01 (d, $J=8.3$ Hz, 4H; o to OH), 4.10 ppm (s, 6H; OCH_3).

Synthesis of compounds 6a, 6b, and 6c: These compounds were synthesized using the same procedure. A representative example is described for **6a**. Compound **5** (0.38 g, 0.9 mmol), monotosylated poly(ethylene glycol) ($M_r=750$, 1.2 g, 2.25 mmol), and excess K_2CO_3 were dissolved in anhydrous acetonitrile (30 mL). The mixture was heated to reflux for 24 h. The resulting solution was poured into water and extracted with dichloromethane. The dichloromethane solution was washed with water, dried over anhydrous magnesium sulfate, and filtered. The solvent was removed with a rotary evaporator, and the crude product was purified by column chromatography (silica gel) using ethyl acetate/methanol (10:1 v/v) to yield a waxy solid (0.77 g, 72%). **6a:** Yield 72%; $^1\text{H NMR}$ (250 MHz, CDCl_3): $\delta=8.75$ (s, 2H; ArH), 8.19 (d, $J=8.4$ Hz; 2Ar-H), 7.75 (d, $J=8.4$ Hz; 2Ar-H), 7.64 (d, $J=8.5$ Hz, 4H; m to OH), 6.89 (d, $J=8.5$ Hz, 4H; o to OH), 4.13 (t, 4H; $\text{CH}_2\text{Ophenyl}$), 3.83 (t, 4H; OCH_2), 3.67–3.38 (m, 128H; OCH_2), 3.29 ppm (s, 6H; OCH_3). **6b:** Yield 69%; $^1\text{H NMR}$ (250 MHz, CDCl_3): $\delta=8.70$ (s, 2H; ArH), 8.11 (d, $J=8.3$ Hz; 2Ar-H), 7.66 (d, $J=8.3$ Hz; 2Ar-H), 7.55 (d, $J=8.4$ Hz, 4H; m to OH), 6.89 (d, $J=8.4$ Hz, 4H; o to OH), 4.01 (t, 4H; $\text{CH}_2\text{Ophenyl}$), 3.57 (t, 4H; OCH_2), 3.51–3.36 (m, 56H; OCH_2), 3.21 ppm (s, 6H; OCH_3). **6c:** Yield 67%; $^1\text{H NMR}$ (250 MHz, CDCl_3): $\delta=8.81$ (s, 2H; ArH), 8.26 (d, $J=8.5$ Hz; 2Ar-H), 7.81 (d, $J=8.5$ Hz; 2Ar-H), 7.69 (d, $J=8.7$ Hz, 4H; m to OCH_2), 6.89 (d, $J=8.7$ Hz, 4H; o to OCH_2), 4.01 (t, 4H; $\text{CH}_2\text{Ophenyl}$), 3.57 (t, 4H; OCH_2), 3.51–3.36 (m, 56H; OCH_2), 3.21 ppm (s, 6H; OCH_3).

Synthesis of compounds 7a, 7b, and 7c: These compounds were synthesized using the same procedure. A representative example is described for **7a**. Ammonium cerium(IV) nitrate (0.188 g, 0.343 mmol) in water (10 mL) was dropped slowly into a solution of compound **6a** (0.19 g, 0.156 mmol) in acetonitrile (10 mL). The reaction mixture was stirred at room temperature for 1 h. The solution was quenched with dichloromethane. Then the resulting solution was washed with water and the dichloromethane solution, dried over anhydrous magnesium sulfate, and filtered. The solvent was removed in a rotary evaporator, and the crude product was purified by column chromatography (silica gel) using ethyl acetate/methanol (10:1 v/v) to yield a waxy solid (0.17 g, 91%). **7a:** Yield 91%; $^1\text{H NMR}$ (250 MHz, CDCl_3): $\delta=8.17$ (m, 4H; ArH), 7.59 (m, 6H; ArH), 7.06 (d, $J=8.7$ Hz, 4H; o to OH), 4.13 (t, 4H; $\text{CH}_2\text{Ophenyl}$), 3.84 (t, 4H; OCH_2), 3.69–3.46 (m, 128H; OCH_2), 3.31 ppm (s, 6H; OCH_3). **7b:** Yield 89%; $^1\text{H NMR}$ (250 MHz, CDCl_3): $\delta=8.22$ (d, $J=8.2$ Hz; 2Ar-H), 8.20 (s, 2H; ArH), 7.63 (m; 6Ar-H), 7.06 (d, $J=8.7$ Hz, 4H; o to OH), 4.21 (t, 4H; $\text{CH}_2\text{Ophenyl}$), 3.90 (t, 4H; OCH_2), 3.75–3.53 (m, 56H; OCH_2), 3.36 ppm (s, 6H; OCH_3). **7c:** Yield 91%; $^1\text{H NMR}$ (250 MHz, CDCl_3): $\delta=8.22$ (d, $J=8.2$ Hz; 2Ar-H), 8.19 (s, 2H; ArH), 7.62 (m; 6Ar-H), 7.06 (d, $J=8.7$ Hz, 4H; o to OCH_2), 4.21 (t, 4H; $\text{CH}_2\text{Ophenyl}$), 3.90 (t, 4H; OCH_2), 3.75–3.53 (m, 56H; OCH_2), 3.36 ppm (s, 6H; OCH_3).

Synthesis of compound 9: 1-(Decyloxy)-4-iodobenzene (650 mg, 1.8 mmol), compound **8** (125 mg, 0.679 mmol), $[\text{Pd}(\text{PPh}_3)_4]$ (116 mg), and CuI (19 mg) were added to a mixture of triethylamine (20 mL) and tetrahydrofuran (10 mL). The mixture was degassed and then stirred at 60°C for 24 h. Solvent was removed in a rotary evaporator and the resulting mixture was poured into water and extracted with dichloromethane. The dichloromethane solution was washed with water, dried over anhydrous magnesium sulfate, and filtered. The crude products were purified by column chromatography (silica gel) using dichloromethane/hexane (1:1 v/v) to yield a yellow solid (0.35 g, 80%). $^1\text{H NMR}$ (250 MHz, CDCl_3): $\delta=7.74$ (s; 2Ar-H), 7.59 (d, $J=8.8$ Hz, 4H; m to OCH_2), 6.90 (d, $J=8.8$ Hz, 4H; o to OCH_2), 3.99 (t, 4H; $\text{CH}_2\text{Ophenyl}$), 1.80 (t, 4H; OCH_2CH_2), 1.48–1.28 (m, 28H; CH_2CH_2), 0.88 ppm (t, 6H; CH_2CH_3).

Synthesis of compound 10: Compound **9** (0.3 g, 0.46 mmol) and lithium aluminum hydride (61 mg, 1.85 mmol) were added to tetrahydrofuran (20 mL). The mixture was heated to reflux for 4 h. Solvent was removed

in a rotary evaporator and the resulting mixture was poured into water and extracted with dichloromethane. The dichloromethane solution was washed with water, dried over anhydrous magnesium sulfate, and filtered. The crude products were purified by column chromatography (silica gel) using dichloromethane/hexane (1:1 v/v) to yield a yellow solid (0.35 g, 80%). $^1\text{H NMR}$ (250 MHz, CDCl_3): $\delta=7.74$ (s; 2Ar-H), 7.45 (d, $J=8.8$ Hz, 4H; m to OCH_2), 6.89 (s; 2Ar-H), 6.86 (d, $J=8.8$ Hz, 4H; o to OCH_2), 3.97 (t, 4H; $\text{CH}_2\text{Ophenyl}$), 1.79 (t, 4H; OCH_2CH_2), 1.46–1.27 (m, 28H; CH_2CH_2), 0.88 ppm (t, 6H; CH_2CH_3).

Synthesis of compounds 1, 2, and 3: These compounds were synthesized using the same procedure. A representative example is described for **1**. A mixture of **10** (97 mg, 0.196 mmol) and **7a** (162 mg, 0.142 mmol) in ethanol (20 mL) and acetic acid (2 mL) was heated to reflux for 2 h. The mixture was cooled to room temperature, poured into water, and extracted with dichloromethane. The dichloromethane solution was washed with water, dried over anhydrous magnesium sulfate, and filtered. The crude products were purified by column chromatography (silica gel) using dichloromethane/methanol (20:1 v/v) as eluent and by preparative HPLC to yield a yellow solid (0.19 g, 53%). **1:** Yield 53%; $^1\text{H NMR}$ (250 MHz, CDCl_3): $\delta=9.47$ (d, $J=8.4$ Hz, 2H), 8.71 (s; 2Ar-H), 7.95 (s; 2Ar-H), 7.93 (d, $J=8.4$ Hz, 2H), 7.73 (m, 8H; m to OCH_2), 7.09 (d, $J=8.7$ Hz, 4H; o to OCH_2), 6.97 (d, $J=8.8$ Hz, 4H; o to OCH_2), 4.23 (t, 4H; $\text{CH}_2\text{Ophenyl}$), 4.02 (t, 4H; OCH_2), 3.92 (t, 4H; $\text{CH}_2\text{Ophenyl}$), 3.78–3.53 (m, 128H), 3.36 (s, 6H; OCH_3), 1.83 (t, 4H; OCH_2CH_2), 1.50–1.29 (m, 28H; CH_2CH_2), 0.89 ppm (t, 6H; CH_2CH_3); $^{13}\text{C NMR}$ (100 MHz, CDCl_3): $\delta=159.7$, 159.0, 142.7, 132.3, 128.8, 126.7, 123.6, 115.6, 115.2, 114.9, 97.9, 86.1, 72.0, 71.0, 69.9, 68.3, 67.7, 59.1, 32.0, 29.7, 29.6, 29.4, 26.2, 22.8, 14.2 ppm; elemental analysis calcd (%) for $\text{C}_{138}\text{H}_{208}\text{N}_2\text{O}_{38}$: C 66.22, H 8.38, N 1.12; found: C 65.86, H 8.62, N 1.00; MALDI-TOF-MS: m/z calcd for $\text{C}_{138}\text{H}_{208}\text{N}_2\text{O}_{38}$: 2503.12 $[\text{M}+\text{H}]^+$; found: 2504.28. **2:** Yield 55%; $^1\text{H NMR}$ (250 MHz, CDCl_3): $\delta=9.47$ (d, $J=8.4$ Hz, 2H), 8.70 (s; 2Ar-H), 7.95 (s; 2Ar-H), 7.93 (d, $J=8.4$ Hz, 2H), 7.74 (m, 8H; m to OCH_2), 7.10 (d, $J=8.6$ Hz, 4H; o to OCH_2), 6.86 (d, $J=8.8$ Hz, 4H; o to OCH_2), 4.24 (t, 4H; $\text{CH}_2\text{Ophenyl}$), 4.02 (t, 4H; OCH_2), 3.94 (t, 4H; $\text{CH}_2\text{Ophenyl}$), 3.78–3.53 (m, 56H), 3.36 (s, 6H; OCH_3), 1.83 (t, 4H; OCH_2CH_2), 1.50–1.29 (m, 28H; CH_2CH_2), 0.89 ppm (t, 6H; CH_2CH_3); $^{13}\text{C NMR}$ (100 MHz, CDCl_3): 159.7, 159.0, 142.6, 132.5, 128.7, 126.7, 123.6, 115.7, 115.2, 114.9, 97.9, 86.2, 72.0, 71.0, 70.7, 68.3, 67.7, 59.1, 32.0, 29.7, 29.6, 29.4, 26.2, 22.8, 14.2 ppm; elemental analysis calcd (%) for $\text{C}_{102}\text{H}_{136}\text{N}_2\text{O}_{20}$: C 71.64, H 8.02, N 1.64; found: C 71.26, H 8.12, N 1.49; MALDI-TOF-MS: m/z calcd for $\text{C}_{102}\text{H}_{136}\text{N}_2\text{O}_{20}$: 1710.17 $[\text{M}+\text{H}]^+$; found: 1710.67. **3:** Yield 54%; $^1\text{H NMR}$ (250 MHz, CDCl_3): $\delta=9.46$ (d, $J=8.4$ Hz, 2H), 8.69 (s; 2Ar-H), 7.95 (s; 2Ar-H), 7.93 (d, $J=8.4$ Hz, 2H), 7.74 (m, 8H; m to OCH_2), 7.10 (d, $J=8.6$ Hz, 4H; o to OCH_2), 6.98 (d, $J=8.8$ Hz, 4H; o to OCH_2), 4.24 (t, 4H; $\text{CH}_2\text{Ophenyl}$), 4.03 (t, 4H; OCH_2), 3.94 (t, 4H; $\text{CH}_2\text{Ophenyl}$), 3.78–3.53 (m, 24H), 3.38 (s, 6H; OCH_3), 1.84 (t, 4H; OCH_2CH_2), 1.49–1.28 (m, 28H; CH_2CH_2), 0.89 ppm (t, 6H; CH_2CH_3); $^{13}\text{C NMR}$ (100 MHz, CDCl_3): 158.2, 156.6, 142.1, 132.1, 128.5, 126.7, 123.6, 115.7, 115.2, 114.9, 97.9, 86.4, 72.7, 71.0, 70.7, 68.9, 59.3, 31.7, 29.4, 29.1, 28.7, 26.2, 22.8, 14.2 ppm; elemental analysis calcd (%) for $\text{C}_{86}\text{H}_{104}\text{N}_2\text{O}_{12}$: C 76.08, H 7.72, N 2.06; found: C 75.87, H 7.86, N 2.12; MALDI-TOF-MS: m/z calcd for $\text{C}_{86}\text{H}_{104}\text{N}_2\text{O}_{12}$: 1358.7 $[\text{M}+\text{H}]^+$, 1380.7 $[\text{M}+\text{Na}]^+$, 1396.7 $[\text{M}+\text{K}]^+$; found: 1358.5 $[\text{M}+\text{H}]^+$, 1379.5 $[\text{M}+\text{Na}]^+$, 1397.5 $[\text{M}+\text{K}]^+$.

Acknowledgements

This work was supported by the National Creative Research Initiative Program of the Korean Ministry of Science and Technology. E.L. and Z.H. acknowledge a fellowship of the BK21 program from the Ministry of Education and Human Resources Development.

[1] J.-M. Lehn, *Proc. Natl. Acad. Sci. USA* **2002**, *99*, 4763–4768.

[2] F. J. M. Hoeben, P. Jonkheijm, E. W. Meijer, A. P. H. J. Schenning, *Chem. Rev.* **2005**, *105*, 1491–1546.

- [3] M. Lee, B.-K. Cho, W.-C. Zin, *Chem. Rev.* **2001**, *101*, 3869–3892.
- [4] a) W.-Y. Yang, J.-H. Ahn, Y.-S. Yoo, N.-K. Oh, M. Lee, *Nat. Mater.* **2005**, *4*, 399–402; b) J.-K. Kim, E. Lee, Z. Huang, M. Lee, *J. Am. Chem. Soc.* **2006**, *128*, 14022–14023; c) A. Ajayaghosh, R. Varghese, S. J. George, C. Vijayakumar, *Angew. Chem.* **2006**, *118*, 1159–1162; *Angew. Chem. Int. Ed.* **2006**, *45*, 1141–1144; d) W. Jin, T. Fukushima, A. Kosaka, M. Niki, N. Ishii, T. Aida, *J. Am. Chem. Soc.* **2005**, *127*, 8284–8285.
- [5] a) J. J. L. M. Cornelissen, M. Fischer, N. A. J. M. Sommerdijk, R. J. M. Nolte, *Science* **1998**, *280*, 1427–1430; b) E. Lee, Y.-H. Jeong, J.-K. Kim, M. Lee, *Macromolecules* **2007**, *40*, 8355–8360.
- [6] a) A. Aggeli, M. Bell, L. M. Carrick, C. W. G. Fishwick, R. Harding, P. J. Mawer, S. E. Radford, A. E. Strong, N. Boden, *J. Am. Chem. Soc.* **2003**, *125*, 9619–9628; b) A. Aggeli, I. A. Nyrkova, M. Bell, R. Harding, L. Carrick, T. C. B. McLeish, A. N. Semenov, N. Boden, *Proc. Natl. Acad. Sci. USA* **2001**, *98*, 11857–11862.
- [7] H. A. Lashuel, S. R. LaBrenz, L. Woo, L. C. Serpell, J. W. Kelly, *J. Am. Chem. Soc.* **2000**, *122*, 5262–5277.
- [8] a) E. R. Zubarev, M. U. Pralle, E. D. Sone, S. I. Stupp, *J. Am. Chem. Soc.* **2001**, *123*, 4105–4106; b) B. W. Messmore, P. A. Sukerkar, S. I. Stupp, *J. Am. Chem. Soc.* **2005**, *127*, 7992–7993.
- [9] a) A. Ajayaghosh, C. Vijayakumar, R. Varghese, S. J. George, *Angew. Chem.* **2006**, *118*, 470–474; *Angew. Chem. Int. Ed.* **2006**, *45*, 456–460; b) J. Bae, J.-H. Choi, Y.-S. Yoo, N.-K. Oh, B.-S. Kim, M. Lee, *J. Am. Chem. Soc.* **2005**, *127*, 9668–9669; c) J.-H. Ryu, H.-J. Kim, Z. Huang, E. Lee, M. Lee, *Angew. Chem.* **2006**, *118*, 5430–5433; *Angew. Chem. Int. Ed.* **2006**, *45*, 5304–5307.
- [10] W.-Y. Yang, E. Lee, M. Lee, *J. Am. Chem. Soc.* **2006**, *128*, 3484–3485.
- [11] a) B. N. Boden, K. J. Jardine, A. C. W. Leung, M. J. MacLachlan, *Org. Lett.* **2006**, *8*, 1855–1858; b) B. A. D. Neto, A. S. A. Lopes, G. Ebeling, R. S. Gonçalves, V. E. U. Costa, F. H. Quina, J. Dupont, *Tetrahedron* **2005**, *61*, 10975–10982; c) Y. Zhu, K. M. Gibbons, A. P. Kul-karni, S. A. Jenekhe, *Macromolecules* **2007**, *40*, 804–813.
- [12] a) M. Kölbl, T. Beyersdorff, X. H. Cheng, C. Tschierske, J. Kain, S. Diele, *J. Am. Chem. Soc.* **2001**, *123*, 6809–6818; b) F. Morle, R. W. Date, D. Guillon, D. W. Bruce, R. L. Finn, C. Wilson, A. J. Blake, M. Schröder, B. Donnio, *Chem. Eur. J.* **2003**, *9*, 2484–2501.
- [13] From the experimental values of volumes of the unit cells (V_{cell}), and the density (ρ), the average number (n) of molecules arranged in a unit cell of the cylinders with a thickness of 4.5 Å (as observed from X-ray diffraction) can be calculated according to following equation, in which M is the molecular mass and N_A is the Avogadro number: $n = V_{\text{cell}}(N_A/M)\rho$.
- [14] a) J.-K. Kim, M.-K. Hong, J.-H. Ahn, M. Lee, *Angew. Chem.* **2005**, *117*, 332–336; *Angew. Chem. Int. Ed.* **2005**, *44*, 328–332; *Angew. Chem. Int. Ed.* **2005**, *44*, 328–332; b) X. Cheng, M. Prehm, M. K. Das, J. Kain, U. Baumeister, S. Diele, D. Leine, A. Blume, C. Tschierske, *J. Am. Chem. Soc.* **2003**, *125*, 10977–10996; c) B. Chen, U. Baumeister, Z. Pelzl, M. K. Das, X. Zeng, G. Ungar, C. Tschierske, *J. Am. Chem. Soc.* **2005**, *127*, 16578–16591.
- [15] J.-H. Ryu, D.-J. Hong, M. Lee, *Chem. Commun.* **2008**, 1043–1054.
- [16] a) Z. Li, M. A. Hillmyer, T. P. Lodge, *Langmuir* **2006**, *22*, 9409–9417; b) G. Guérin, J. Ruez, I. Manners, M. A. Winnik, *Macromolecules* **2005**, *38*, 7819–7827.
- [17] a) J. P. Hill, W. Jin, A. Kosaka, T. Fukushima, H. Ichihara, T. Shimomura, K. Ito, T. Hashizume, N. Ishii, T. Aida, *Science* **2004**, *304*, 1481–1483; b) G. John, M. Masuda, Y. Okada, K. Yase, T. Shimizu, *Adv. Mater.* **2001**, *13*, 715–718.
- [18] a) C. Tan, M. R. Pinto, M. E. Kose, I. Ghiviriga, K. S. Schanze, *Adv. Mater.* **2004**, *16*, 1208–1212; b) X. Zhang, Z. Chen, F. Würthner, *J. Am. Chem. Soc.* **2007**, *129*, 4886–4887; c) A. P. H. J. Schenning, A. F. M. Kilbinger, F. Biscarini, M. Cavallini, H. J. Cooper, P. J. Derrick, W. J. Feast, R. Lazzaroni, Ph. Leclère, L. A. McDonnell, E. W. Meijer, S. C. J. Meskers, *J. Am. Chem. Soc.* **2002**, *124*, 1269–1275.
- [19] a) A. P. H. J. Schenning, P. Jonkheijm, E. Peeters, E. W. Meijer, *J. Am. Chem. Soc.* **2001**, *123*, 409–416; b) A. Ajayaghosh, V. K. Praveen, *Acc. Chem. Res.* **2007**, *40*, 644–656; c) E. G. McRae, M. J. Kasha, *J. Chem. Phys.* **1958**, *28*, 721–722; d) D. G. Whitten, *Acc. Chem. Res.* **1993**, *26*, 502–509.
- [20] a) R. L. B. Selinger, J. V. Selinger, A. P. Malanoski, J. P. Schnur, *Phys. Rev. Lett.* **2004**, *93*, 158103; b) A. Brizard, C. Aimé, T. Labrot, I. Huc, D. Berthier, F. Artzer, B. Desbat, R. Oda, *J. Am. Chem. Soc.* **2007**, *129*, 3754–3762; c) C. W. G. Fishwick, A. J. Beevers, L. M. Carrick, C. D. Whitehouse, A. Aggeli, N. Boden, *Nano Lett.* **2003**, *3*, 1475–1479.
- [21] J.-H. Ryu, E. Lee, Y.-b. Lim, M. Lee, *J. Am. Chem. Soc.* **2007**, *129*, 4808–4814.

Received: April 8, 2008

Published online: July 4, 2008